



Weak layer fracture: facets and depth hoar

I. Reiweger and J. Schweizer

WSL Institute for Snow and Avalanche Research SLF, Davos, Switzerland

Correspondence to: I. Reiweger (reiweger@slf.ch)

Received: 22 April 2013 – Published in The Cryosphere Discuss.: 3 May 2013

Revised: 22 July 2013 – Accepted: 6 August 2013 – Published: 23 September 2013

Abstract. Understanding failure initiation within weak snow layers is essential for modeling and predicting dry-snow slab avalanches. We therefore performed laboratory experiments with snow samples containing a weak layer consisting of either faceted crystals or depth hoar. During these experiments the samples were loaded with different loading rates and at various tilt angles until fracture. The strength of the samples decreased with increasing loading rate and increasing tilt angle. Additionally, we took pictures of the side of four samples with a high-speed video camera and calculated the displacement using a particle image velocimetry (PIV) algorithm. The fracture process within the weak layer could thus be observed in detail. Catastrophic failure started due to a shear fracture just above the interface between the depth hoar layer and the underlying crust.

1 Introduction

Most skier-triggered dry-snow slab avalanches release due to the failure of a weak layer consisting of depth hoar, faceted crystals, or surface hoar crystals (Schweizer and Jamieson, 2001). A macroscopic crack ($\mathcal{O}(10\text{ cm})$ or more) in the weak layer underlying a cohesive slab might lead to crack propagation and eventually to the release of a slab avalanche (Schweizer et al., 2003). The initial failure and its extension to the critical crack size leading to fast crack propagation is still not fully understood.

Heierli et al. (2008) suggested avalanche initiation to be modeled as a mixed-mode anticrack where the main mechanism behind weak layer failure is collapse of the weak layer. Other authors such as McClung (1979, 2009) or Bažant et al. (2003) suggest that the layer first fails in shear.

Previous laboratory studies on the mechanical behavior of snow mainly used displacement-controlled shear exper-

iments. Most experiments were made with homogeneous snow (e.g. McClung, 1977; de Montmollin, 1982; Schweizer, 1998). Those studies showed that snow is a pressure-sensitive and strain-softening material, the latter was assumed to be a consequence of sintering processes inside the snow during deformation (e.g. Colbeck, 1998; Reiweger et al., 2009b). In addition, it was shown that snow strength decreases with increasing rate of displacement (Narita, 1980).

Weak snow layers were tested in the field (Föhn et al., 1998; Jamieson and Johnston, 2001) as well as in the laboratory (Fukuzawa and Narita, 1993; Joshi et al., 2006; Reiweger and Schweizer, 2010; Walters et al., 2010; Walters and Adams, 2012). The laboratory studies showed that the deformation subjected to snow samples was concentrated in the weak layer, which provides a preferential plane for shear failure. In the experiments we performed with samples containing a weak layer of surface hoar (Reiweger and Schweizer, 2010) we found that at least this kind of weak layer failed in shear more likely than in compression.

We performed loading experiments with snow samples containing a weak depth hoar layer with a new loading apparatus especially designed for studying the (initial) failure of snow with respect to avalanche release; due to the small sample size we cannot study fracture propagation. In order to obtain loading conditions similar to those in nature, the samples were loaded by a combination of shear and normal load depending on the tilt angle. A detailed description of our loading apparatus is given in Reiweger et al. (2010).

2 Methods

2.1 Snow samples and loading experiments

The snow samples containing a weak layer were either natural samples taken from the field (samples B, Table 1) or

Table 1. Characteristics of the different snow samples tested. Snow type is described as grain type according to Fierz et al. (2009), average grain size (in mm), and hand hardness index, while N denotes the number of successful experiments performed with each type of sample.

Sample layering	Density (kg m^{-3})	Thickness (mm)	Length \times Width (mm)	Snow type	N
rounded grains	225	35	120×90	RG, 0.25, 1–2	8
depth hoar TRA		0.2		FC(DH), 1–1.5, 1	
rounded grains		40		RG, 0.25, 1–2	
rounded grains	190	35	120×90	RG, 0.5, 2	4
faceted crystals LAY		0.2		FC(FCxr), 0.75, 1	
rounded grains		35		RG, 0.5, 2	
rounded grains	200	40	200×100	RG(FC), 0.25–1.5, 2–3	17
depth hoar B		50		DH(FC), 1.25–3, 1	
melt-freeze crust		20		MFcr, 1–2, 4	

artificial samples (samples TRA and LAY, Table 1) produced in the laboratory. The natural samples were carefully cut out from the snow cover on the study plot behind the SLF with a snow saw and directly carried to the laboratory. The artificial weak layers of faceted crystals and depth hoar were grown by applying a strong vertical temperature gradient to a layered snow sample. The snow samples for growing faceted crystals consisted of a layer of low-density snow (fresh new snow crystals produced by a snow machine; Schleef et al., 2013) sandwiched between two dense snow layers ($\rho \approx 300 \text{ kg m}^{-3}$), produced by sieving new snow into a box, compressing it and letting it sinter for 48 h. A detailed description of this procedure is given in Reiweger et al. (2010), and the layering of the samples is shown in Table 1. The weak layer in the artificial samples was a thin layer of faceted crystals, whereas the natural samples contained a thick weak layer of large depth hoar crystals.

The loading experiments were performed at a temperature of -5°C with the apparatus shown in Fig. 1 and described by Reiweger et al. (2010). Loading rates varied between 10 Pa s^{-1} and 400 Pa s^{-1} . Samples were tilted (0 – 35°) in order to mimic a “slope angle” α and loaded via the gravitational force. The normal and tangential load were thus given by $F \cdot \cos \alpha$ and $F \cdot \sin \alpha$, respectively. The weight of the upper sample holder was compensated.

2.2 Particle image velocimetry

In order to monitor the displacement field on the sides of our samples we took photos during the measurements. These photos were then analyzed with a particle image velocimetry algorithm (PIV). The PIV algorithm recognizes patterns on a photograph taken from the snow sample and tracks them over various subsequent photographs. The snow sample was sprayed with paint to achieve sufficient contrast for the PIV algorithm to find a pattern. Assuming plane strain conditions, the displacement field on the side of the sample should be representative for the displacement field also within the sam-

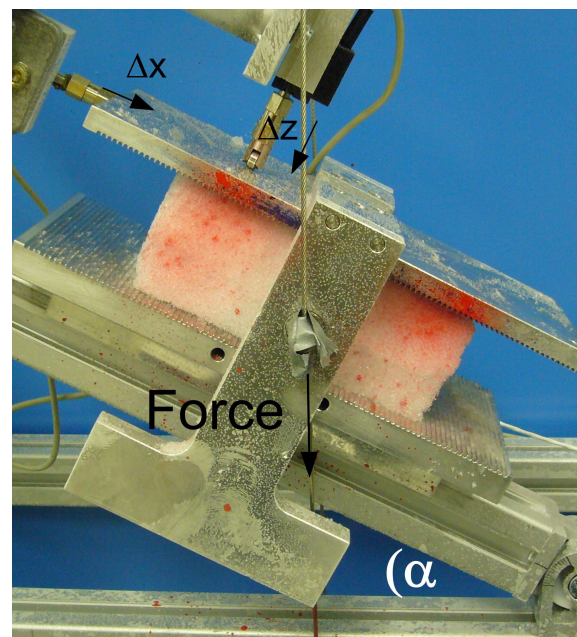


Fig. 1. Snow sample in loading apparatus. Δx and Δz denote the shear and normal displacement, α denotes the tilt angle (Reiweger et al., 2010).

ple. In a set of validation experiments the accuracy of the displacement calculated by the PIV algorithm was found to be $\pm 0.01 \text{ mm}$. A detailed description of the PIV algorithm can be found in Roesgen and Totaro (1995); its application to snow is described in Reiweger et al. (2009a). For the fast experiments with samples B8, B9, B10, and B17, we acquired images at a high rate with a high-speed video camera (camera type VDS Vosskühler HCC-1000, resolution 1024 by 512 pixels, recording rate 300 frames per second). Since the weak layer B was several centimeters thick we could observe what was happening within the weak layer shortly before and during fracture.

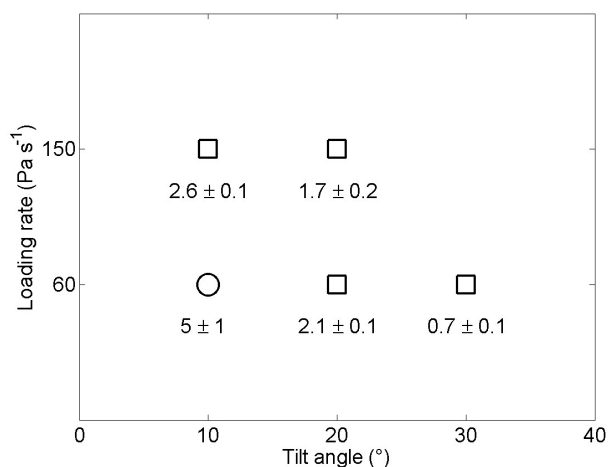


Fig. 2. Strength in kPa for samples TRA and LAY as function of tilt angle and loading rate ($N = 11$). The squares represent fracture, the circle indicates the one sample that did not fracture at this tilt angle and loading rate.

3 Results

3.1 Strength

We performed 29 experiments with three sample types for various loading rates. The load needed to fracture the samples was measured. Detailed results of all measurements can be found in Table 2.

Figure 2 shows the strength for samples of types TRA and LAY as function of tilt angle and loading rate. Due to the limited number of experiments for each loading rate and tilt angle, we calculated the standard deviation with a bootstrap algorithm (Davison and Hinkley, 1997), using 2000 sample data sets. It can be seen that strength decreases with increasing tilt angle (Fig. 4) and increasing loading rate. For samples TRA and LAY both these trends are clearly larger than the standard deviation.

For samples of type B (Fig. 3) the decrease of strength with increasing tilt angle and loading rate is still apparent – as the highest strength values are clearly found at a tilt angle of 0° – but not as obvious, since the strength differences between 25° and 35° are of the same order of magnitude as the standard deviation (again calculated with the bootstrap algorithm). Comparing the measurements below and above a loading rate of 150 Pa s^{-1} , however, the decrease with strength with increasing loading rate remains evident.

3.2 Fracture behavior

The fracture of samples B8, B9, B10, and B17 was monitored with a high-speed video camera. The images from the high-speed videos were again analyzed with the particle image velocimetry (PIV) algorithm. Detailed results are given for

Table 2. Overview of all successful measurements. α , $\dot{\sigma}$, and σ_c denote the slope angle, the loading rate, and the sample strength, respectively.

Sample	α ($^\circ$)	$\dot{\sigma}$ (Pa s^{-1})	σ_c (kPa)
TRA1	20	60	2.1
TRA2	20	150	1.9
TRA3	30	60	0.5
TRA4	30	60	0.8
TRA5	20	60	2.1
TRA6	20	150	1.1
TRA7	20	150	2.4
TRA8	20	150	1.5
LAY1	10	150	2.5
LAY2	10	60	5.3
LAY3	10	150	2.6
LAY4	10	60	> 10
B1	25	42	1.6
B2	25	200	0.7
B3	25	84	2.4
B4	25	9	2.3
B5	25	14	2.0
B6	35	10	3.8
B7	35	200	1.0
B8	35	200	1.2
B9	35	18	1.7
B10	35	20	0.8
B11	0	444	2.7
B12	0	439	2.5
B13	0	30	2.5
B14	0	15	2.5
B15	25	290	1.3
B16	0	42	6.0
B17	25	220	1.7

sample B9, which was loaded with a loading rate of 18 Pa s^{-1} at a tilt angle of 35° (Table 2).

For the PIV analysis we chose two different sections of the snow sample, i.e. an upper rectangle (dimensions $22 \text{ mm} \times 87 \text{ mm}$, Fig. 5a) where a local fracture happened and a lower rectangle (dimensions $16 \text{ mm} \times 64 \text{ mm}$, Fig. 5b) where the catastrophic fracture of the whole sample commenced. The arrows in Fig. 5 mark those two fracture locations. The weak layer is approximately located between the two red lines (Fig. 5a). Analysis of the 33 images before and after the onset of the final crack allowed us to exactly follow the fracture process. The PIV results show the displacement between the first of the 33 images and image i , where $i = 2, \dots, 33$. The time difference between two subsequent images was $1/300 \text{ s}$, and the displacement was averaged across the width of the rectangles shown in Fig. 5. The first series of PIV results shown in Fig. 6 shows the displacement caused by the local fracture within the upper rectangle

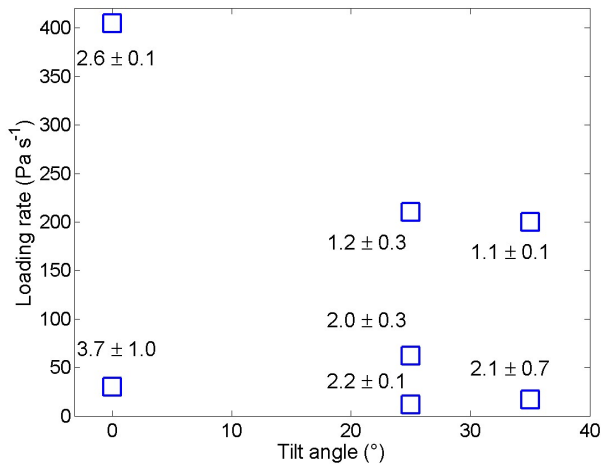


Fig. 3. Strength in kPa for samples of type B as function of tilt angle and loading rate ($N = 17$).

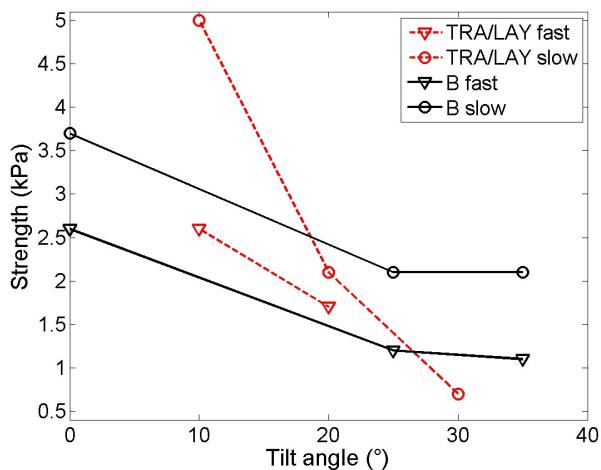


Fig. 4. Strength in kPa for sample types TRA/LAY and B over tilt angle for different loading rates ($N = 28$).

(Fig. 5a). The parallel arrows in the middle of the displacement fields indicate that the catastrophic failure has started, as the snow starts moving to the right and downwards as a cohesive block (Fig. 8a). The seemingly chaotic and even upward movement during fracture (Fig. 6) reflects the layer being crushed and pieces of snow being pressed out of the sample sideways. The second series of images (Fig. 7) shows the PIV results of the onset of the final crack within the lower rectangle (Fig. 5b). At image 29 we see the onset of the catastrophic shear fracture, the upper arrows pointing forward, the lower arrows pointing backward. The image of sample B9 0.3 s after the image shown in Fig. 5 (which were taken 0.01 s before the first local failure at the top of the sample appeared) is displayed in Fig. 8b. The upper and lower parts of the sample are still fairly intact, but the weak layer is squashed and the snow has crumbled away sideways. The final image of

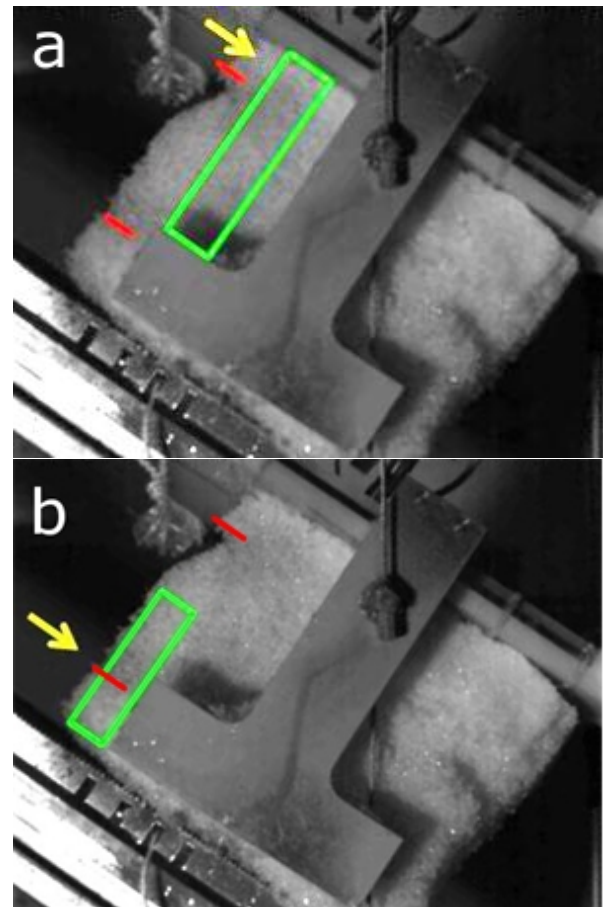


Fig. 5. (a) Section (green rectangle) where first local failure occurred. (b) Section where the crack propagation started. The red lines mark the position of the weak layer. Sample B9.

the high speed camera sequence (Fig. 8c), taken 1 s after the images in Fig. 5, shows the sample holders after the samples has fractured catastrophically. The movies taken during the experiments with samples B8, B10, and B17 showed similar behavior.

4 Discussion

When testing samples including a weak layer, the sample geometry and loading conditions are often not perfect. Natural depth hoar samples are especially difficult to harvest, since, in contrast to layers of buried surface hoar, they are usually at the bottom of the snowpack and hardly ever have a cohesive layer beneath them. In the case of samples of kind B, we were lucky to have a crust below the depth hoar layer, which made it possible to cut and transport samples. The height of the samples had to be chosen quite large for the reason of keeping the crust at the bottom. We are aware that this gives an unfavorable area to height ratio for the whole sample.

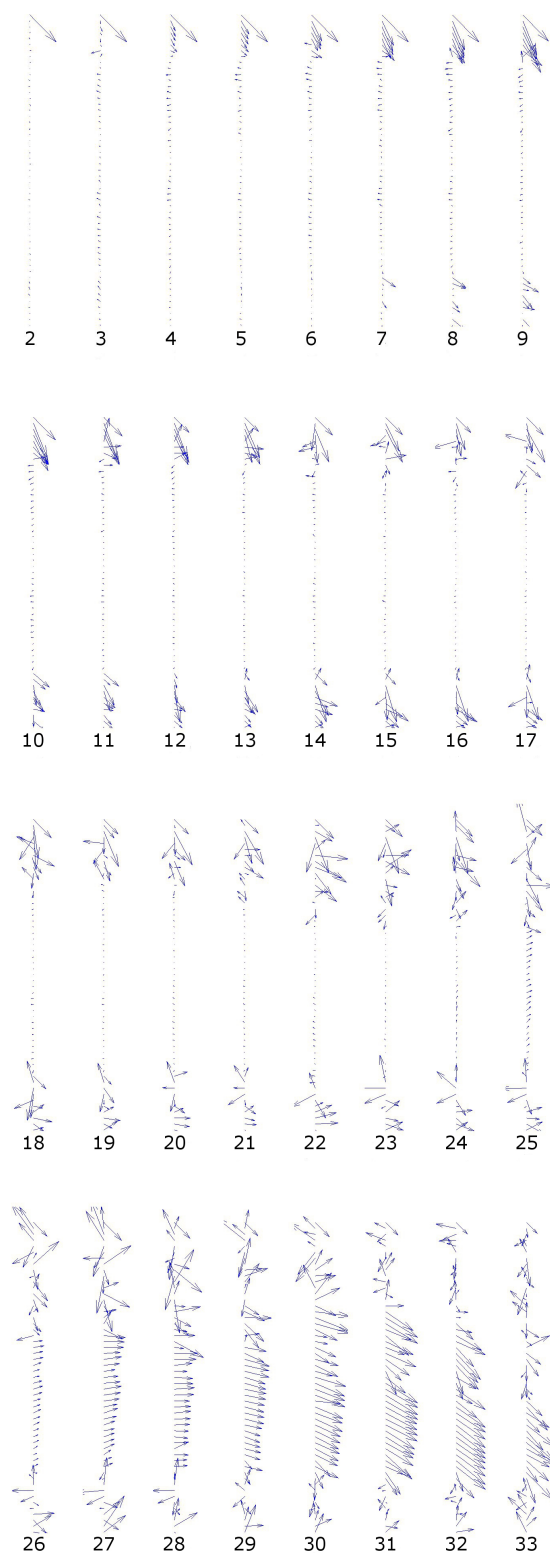


Fig. 6. Horizontally averaged displacement field within the upper rectangle (Fig. 5a) during the failure process of sample B9. The displacement is shown between image 1 and images 2–33, respectively. The uppermost arrow in each sequence is only for reference, its coordinates are [0.8 mm, 0.8 mm]. The time difference between subsequent images was 1/300 s.

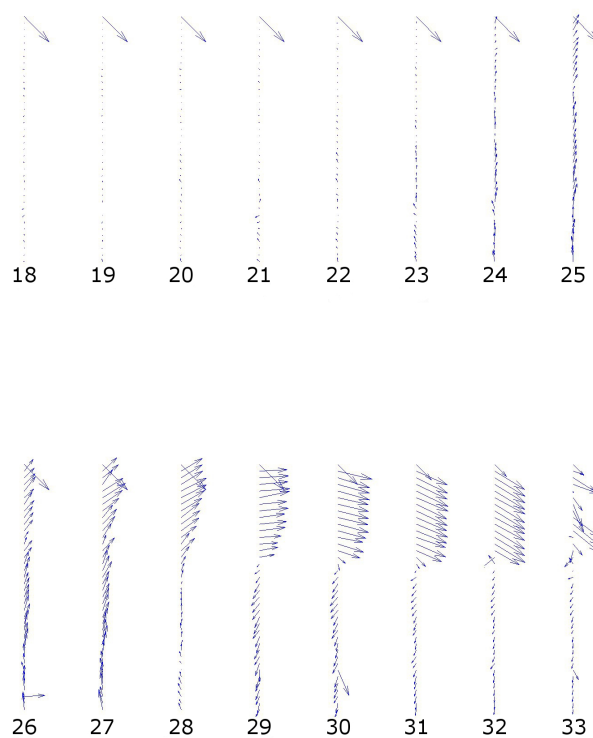


Fig. 7. Averaged displacement field within the lower rectangle during the initiation of the catastrophic fracture (Fig. 5b) of sample B9. Displacement is shown between image 1 and images 18–33. Again uppermost arrow for reference, coordinates [0.8 mm, 0.8 mm] (same as in Fig. 6).

The artificial samples had a thin weak layer, which improved the area to height ratio, especially since for layered samples the deformation is concentrated within the weak layer (Reiweger et al., 2009a; Reiweger and Schweizer, 2010). For the artificial samples TRA and LAY we found a strong decrease of sample strength with increasing tilt angle, suggesting a failure in shear rather than in compression. The measurements with the natural samples B showed this trend as well, though less prominent. We assume that this is due to the height of the samples, which was unfavorably high compared to the sample area, as discussed above.

The well-known (Fukuzawa and Narita, 1993; Schweizer, 1998) rate dependence of snow strength was reproduced well for all our samples, i.e. sample strength decreased with increasing loading rate. The absolute strength of the samples might be higher than the strength of a similar weak layer in a natural snowpack due to the finite size of the (relatively small) samples (Bažant and Pang, 2007). The tendency, i.e. the strength decrease, should not be affected by size effect, however, and can therefore be assumed to be valid also for natural weak layer in the field.

The high-speed video images from the fracture of samples B9 show that a small fracture occurred at an arbitrary place within the weak layer, and this fracture then triggered a shear

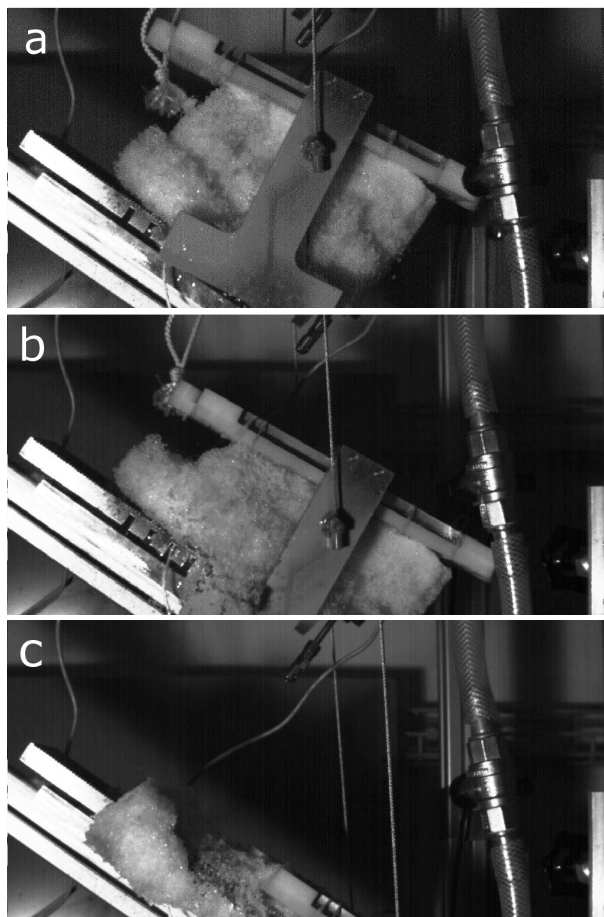


Fig. 8. Sample B9, during catastrophic failure. The images (b) and (c) were taken 0.1 s and 0.9 s after image (a), respectively.

crack at the interface between the weak layer and the crust at the bottom. This crack spread through the whole sample (in x direction, Fig. 1) and caused the sample to fail catastrophically. A similar fracture mechanism was observed for all four samples which were filmed with the high-speed camera. These observations might be specific to our thick samples of natural depth hoar.

The movies from samples B8, B9, B10, and B17 are unique in showing the actual formation of the catastrophic fracture of a weak depth hoar layer. All four movies suggest that the catastrophic fracture started as a shear fracture (Fig. 7, image 29) at the interface of the depth hoar layer and the crust below the layer. This catastrophic failure was triggered by some disturbance somewhere within the weak layer, maybe at a point where the weak layer had a particularly weak spot due to the inherent small-scale inhomogeneity of snow layers. During fracture the samples then collapsed completely (Fig. 8).

A prerequisite for avalanche release is an initial crack, and its formation from diffuse damage is labeled “failure initiation”. Once the initial crack reaches its critical size it prop-

agates across and up and down the slope (“crack propagation”) thus leading to the release of an avalanche (Schweizer et al., 2003). Recently, crack propagation propensity has been studied with field experiments (Gauthier and Jamieson, 2008; Schweizer et al., 2011; Sigrist and Schweizer, 2007; van Herwijnen et al., 2010). The weak layer in an elongated snow column is cut with a saw (so that the overlying slab slightly bends) until a self-propagating crack starts. These experiments can well be interpreted with the numerical solution by Heierli et al. (2008).

Within our present experiments we only studied fracture initiation, since self-propagation cracks were not observed within our relatively small (maximum length 20 cm) samples. This is in accordance with observations (McClung, 2011) and theoretical predictions (Heierli et al., 2008) which indicate that critical lengths are often greater than 20 cm.

Field studies on the influence of slope angle on snow failure reveal ambiguous results, albeit all trends are small. Jamieson (1999) found a stability decrease with increasing slope angle studying compression test (CT) results, in agreement with the evaluation of Rutschblock (RB) tests at different slope angles by Campbell and Jamieson (2007). On the other hand, Heierli et al. (2011) and Bair et al. (2012) reported increasing extended column test (ECT) score with increasing slope angle.

5 Conclusions

We performed 29 loading experiments with samples containing a weak layer of either facets or depth hoar to study failure initiation but not crack propagation. Sample strength decreased with increasing loading rate and tilt angle. The decrease in strength with increasing tilt angle suggests that facets and depth hoar are more prone to failure in shear than to failure in compression, as was previously shown for samples containing a weak layer of surface hoar (Reiweger and Schweizer, 2010). For natural avalanche release this means that steep terrain favors the damage process leading to the formation of an initial crack.

During the experiments with the thick depth hoar samples we could actually follow how the initial failure started. It seemed to start as a local failure at a seemingly arbitrary position within the weak layer, which induced a shear crack at the weak interface between the depth hoar layer and the crust below. So the inherent disordered nature of snow seems to be important for failure initiation, and a weak layer or weak interface is needed where a macroscopic crack, which can grow large enough for crack propagation, can form.

Supplementary material related to this article is available online at <http://www.the-cryosphere.net/7/1447/2013/tc-7-1447-2013-supplement.zip>.

Acknowledgements. We thank Stephan Simioni, Susanna Hoinkes, and Klemens Mayer for help with the experiments. We are grateful for comments by the Editor F. Dominé and two anonymous reviewers that helped improving the paper.

Edited by: F. Dominé

References

- Bair, E. H., Simenhois, R., Birkeland, K., and Dozier, J.: A field study on failure of storm snow slab avalanches, *Cold Reg. Sci. Technol.*, 79–80, 20–28, 2012.
- Bažant, Z. and Pang, S.-D.: Activation energy based extreme value statistics and size effect in brittle and quasibrittle fracture, *J. Mech. Phys. Solids*, 55, 91–131, 2007.
- Bažant, Z., Zi, G., and McClung, D.: Size effect law and fracture mechanics of the triggering of dry snow slab avalanches, *J. Geophys. Res.*, 108, 2119, doi:10.1029/2002JB001884, 2003.
- Campbell, C. and Jamieson, B.: Spatial variability of slab stability and fracture characteristics within avalanche start zones, *Cold Reg. Sci. Technol.*, 47, 134–147, 2007.
- Colbeck, S.: Sintering in a dry snow cover, *J. Appl. Phys.*, 84, 4585–4589, doi:10.1063/1.368684, 1998.
- Davison, A. and Hinkley, D.: *Bootstrap Methods and Their Application*, Cambridge University Press, Cambridge, 1997.
- de Montmollin, V.: Shear tests on snow explained by fast metamorphism, *J. Glaciol.*, 28, 187–198, 1982.
- Fierz, C., Armstrong, R., Durand, Y., Etchevers, P., Greene, E., McClung, D., Nishimura, K., Satyawali, P., and Sokratov, S.: The International Classification for Seasonal Snow on the Ground, Paris, UNESCO-International Hydrological Program (IHP-VII Technical Documents in Hydrology), 83, 90 pp., 2009.
- Föhn, P., Camponovo, C., and Krüsi, G.: Mechanical and structural properties of weak snow layers measured in situ, *Ann. Glaciol.*, 26, 1–6, 1998.
- Fukuzawa, T. and Narita, H.: An experimental study on the mechanical behavior of a depth hoar layer under shear stress, in: *Proceedings International Snow Science Workshop, Breckenridge, Colorado, USA, 4–8 October 1992*, 171–175, 1993.
- Gauthier, D. and Jamieson, B.: Evaluation of a prototype field test for fracture and failure propagation propensity in weak snowpack layers, *Cold Reg. Sci. Technol.*, 51, 87–97, 2008.
- Heierli, J., Gumbsch, P., and Zaiser, M.: Anticrack nucleation as triggering mechanism for snow slab avalanches, *Science*, 321, 240–243, 2008.
- Heierli, J., Birkeland, K., Simenhois, R., and Gumbsch, P.: Anticrack model for skier triggering of slab avalanches, *Cold Reg. Sci. Technol.*, 65, 372–381, 2011.
- Jamieson, J. B.: The compression test – after 25 years, *The Avalanche Review*, 18, 10–12, 1999.
- Jamieson, J. B. and Johnston, C. D.: Evaluation of the shear frame test for weak snowpack layers, *Ann. Glaciol.*, 32, 59–69, 2001.
- Joshi, S. K., Mahajan, P., and Upadhyay, A.: Study of layered snow under shear and tension, in: *Proceedings ISSW 2006. International Snow Science Workshop*, edited by: Gleason, A., Telluride, Colorado, USA, 1–6 October 2006, 165–173, 2006.
- McClung, D.: Direct simple shear tests on snow and their relation to slab avalanche formation, *J. Glaciol.*, 19, 101–109, 1977.
- McClung, D.: Shear fracture precipitated by strain-softening as a mechanism of dry slab avalanche release, *J. Geophys. Res.*, 84, 3519–3526, 1979.
- McClung, D.: Dry snow slab quasi-brittle fracture initiation and verification from field tests, *J. Geophys. Res.*, 114, F01022, doi:10.1029/2007JF000913, 2009.
- McClung, D.: The critical size of macroscopic imperfections in dry snow slab avalanche initiation, *J. Geophys. Res.*, 116, F03003, doi:10.1029/2010JF001866, 2011.
- Narita, H.: Mechanical behaviour and structure of snow under uniaxial tensile stress, *J. Glaciol.*, 26, 275–282, 1980.
- Reiweger, I. and Schweizer, J.: Failure of a layer of buried surface hoar, *Geophys. Res. Lett.*, 37, L24501, doi:10.1029/2010GL045433, 2010.
- Reiweger, I., Ernst, R., Schweizer, J., and Dual, J.: Force-controlled shear experiments with snow samples, in: *Proceedings International Snow Science Workshop*, edited by: Schweizer, J. and van Herwijnen, A., Davos, Switzerland, 27 September–2 October 2009, 120–123, 2009a.
- Reiweger, I., Schweizer, J., Dual, J., and Herrmann, H.: Modelling snow failure with a fibre bundle model, *J. Glaciol.*, 55, 997–1002, 2009b.
- Reiweger, I., Schweizer, J., Ernst, R., and Dual, J.: Load-controlled test apparatus for snow, *Cold Reg. Sci. Technol.*, 62, 119–125, 2010.
- Roesgen, T. and Totaro, R.: Two-dimensional on-line particle imaging velocimetry, *Exp. Fluids*, 19, 188–193, 1995.
- Schleef, S., Jaggi, M., Löwe, H., and Schneebeli, M.: An improved machine to produce nature-identical snow in the laboratory, *J. Glaciol.*, in review, 2013.
- Schweizer, J.: Laboratory experiments on shear failure of snow, *Ann. Glaciol.*, 26, 97–102, 1998.
- Schweizer, J. and Jamieson, J. B.: Snow cover properties for skier triggering of avalanches, *Cold Reg. Sci. Technol.*, 33, 207–221, 2001.
- Schweizer, J., Jamieson, J. B., and Schneebeli, M.: Snow avalanche formation, *Rev. Geophys.*, 41, 1016, doi:10.1029/2002RG000123, 2003.
- Schweizer, J., van Herwijnen, A., and Reuter, B.: Measurements of weak layer fracture energy, *Cold Reg. Sci. Technol.*, 69, 139–144, 2011.
- Sigrist, C. and Schweizer, J.: Critical energy release rates of weak snowpack layers determined in field experiments, *Geophys. Res. Lett.*, 34, L03502, doi:10.1029/2006GL028576, 2007.
- van Herwijnen, A., Schweizer, J., and Heierli, J.: Measurement of the deformation field associated with fracture propagation in weak snowpack layers, *J. Geophys. Res.*, 115, F03042, doi:10.1029/2009JF001515, 2010.
- Walters, D. J. and Adams, E. E.: Directional mechanical properties of radiation recrystallized snow layers from experimental testing, in: *Proceedings International Snow Science Workshop*, edited by: Johnson, J. and Conway, H., Anchorage, Alaska, USA, 16–21 September 2012, 201–208, 2012.
- Walters, D. J., Adams, E. E., Staron, P. J., and McKittrick, L. R.: Shear deformation of radiation recrystallized near surface facets, in: *Proceedings International Snow Science Workshop*, edited by: Osterhuber, R., Lake Tahoe, CA, USA, 17–22 October 2010, 80–87, 2010.